SAND80-1363
Unlimited Release
UC-4

Reaction Rates of Atmospheric Gases With Lithium(Silicon) Alloy

Jimmie Q. Searcy, Fred W. Reinhardt

Sandia National Laboratories

2900-Q(3-80)

Issued by Sandia National Laboratories, operated for the United States Department of Energy by Sandia Corporation.

NOTICE: This report was prepared as an account of work sponsored by an agency of the United States Government. Neither the United States Government nor any agency thereof, nor any of their employees, nor any of their contractors, subcontractors, or their employees, makes any warranty, express or implied, or assumes any legal liability or responsibility for the accuracy, completeness, or usefulness of any information, apparatus, product, or process disclosed, or represents that its use would not infringe privately owned rights. Reference herein to any specific commercial product, process, or service by trade name, trademark, manufacturer, or otherwise, does not necessarily constitute or imply its endorsement, recommendation, or favoring by the United States Government, any agency thereof or any of their contractors or subcontractors. The views and opinions expressed herein do not necessarily state or reflect those of the United States Government, any agency thereof or any of their contractors or subcontractors.

Printed in the United States of America

Available from
National Technical Information Service
U. S. Department of Commerce
5285 Port Royal Road
Springfield, VA 22161

NTIS price codes
Printed copy: $6.00
Microfiche copy: A01

SAND80-1363
Unlimited Release
Printed December 1980

Distribution
Category UC-4

REACTION RATES OF ATMOSPHERIC GASES WITH LITHIUM(SILICON) ALLOY

Jimmie Q. Searcy
Fred W. Reinhardt
Exploratory Batteries Division 2523
Sandia National Laboratories
Albuquerque, NM 87185

ABSTRACT

Reaction rates of small pellets of Li(Si) alloy with atmospheric gases were studied as a prerequisite to specifying how this alloy should be handled during the production of thermal batteries. The results indicate that Li(Si) reacts with oxygen and nitrogen at ambient conditions too slowly to be of concern, but it reacts very rapidly with water vapor. Rate expressions and constants are developed that allow calculating the weight gain of Li(Si) after its reaction with water vapor, and calculated values are given for three water-vapor concentrations that typify those used in dry rooms where thermal batteries are produced.

ACKNOWLEDGMENTS

The authors thank G. C. Nelson (Division 5823) who examined Li(Si) samples with various surface analytical instruments and P. A. Neiswander (Division 2523) who prepared samples for Nelson's analyses and generated the weight-gain data for the 10 cm^2 Li(Si) pellets described in Section 6.

CONTENTS

	Page
1. Introduction	7
2. Experimental Procedure	8
3. Applicable Reaction-Rate Models	12
4. Data Analysis	18
5. Results	22
6. Discussion	27
7. Conclusions	31
References	31
APPENDIX A -- List of Variables	33
APPENDIX B -- Tables of Data and Results	37

ILLUSTRATIONS

Figure		
1	Reaction Volume	9
2	The Gas-Flow System Used to Generate Known Concentrations of Water Vapor in Various Carrier Gases	10
3	Shrinking Core Model With a Solid Core	14
4	Data For a Pellet Exposed to 4.26×10^{-7} g/cm^3 Water Vapor in Argon Carrier Gas at 100°C	19
5	Plot of $\ln(k'_{r,t=0})$ vs $10^3/T$ for the Data Generated With Oxygen Gas; No Water Vapor Added	23
6	Plot of $\ln(k'_{r,t=0})$ vs $10^3/T$ for the Data Generated With Nitrogen Gas; No Water Vapor Added	24
7	Plot of $\ln(k_r)$ vs $10^3/T$ for All Water-Vapor Data	25
8	Plot of k_s vs $T^{1/2}$	26
9	Calculated Curves for the Weight Gain per cm^2 of Li(Si) Pellet Exposed to Varying Water-Vapor Concentrations	30

REACTION RATES OF ATMOSPHERIC GASES WITH LITHIUM(SILICON) ALLOY

1. Introduction

Sandia National Laboratories designs thermal batteries that use lithium(silicon) as an anode alloy. In order to ensure high reliability and long shelf life of the batteries, restrictions must be placed on how battery materials are handled and stored. A knowledge of how battery materials react with gases in ambient air is needed for determining what exposure can be allowed during handling and storage. This report details a study for determining the rates of reaction of Li(Si) alloy with gases in ambient air and develops information that allows calculation of the amount of this reaction during battery production. The alloy used was 44 wt% lithium; the gases studied were oxygen, nitrogen, and water vapor. Rate data were determined by measuring weight gain of Li(Si) samples with a thermogravimetric analyzer (TGA).

Pure lithium is known to react with nitrogen, oxygen, and water vapor,[1] but it also reacts with its own hydroxide to release hydrogen. It has been reported that the reaction of lithium with nitrogen is catalyzed by the presence of water.[1] Lithium oxide reacts with carbon dioxide to give lithium carbonate, and lithium nitride reacts with water to give lithium oxide (or hydroxide, if enough water is available) and ammonia.

A search of the literature yielded no information about the reactivity of Li(Si) alloy with atmospheric gases. Since the electrical potential of Li(Si) measured against that of pure lithium is positive,[2] it follows that the chemical potential of lithium in the alloy is less than that of pure lithium. Therefore, the Li(Si) alloy would not necessarily react as vigorously as pure lithium.

In this work individual data points were not always replicated because our objective was to obtain practical information as soon as possible. Further, the accuracy of these data depends on several assumptions that were not verified during the study. The results obtained are nevertheless self-consistent, and the resulting rate equations are quite adequate for their intended use in specifying procedures for production handling and storage.

Li(Si) alloy, used in thermal batteries as pellets of pressed powder, is exposed to air both in powder and pressed-pellet form. Since it is very difficult to obtain meaningful reaction rates by using irregular-sized powder samples, data in this work were generated by using only small pressed pellets with a known geometry.

The report is divided into several sections. Section 2 describes the experimental procedure, the apparatus used, and how the concentration of water vapor was determined. Section 3 develops the reaction-rate models used with the data to determine rate constants. Since use of the rate models requires calculation of several factors that are dependent on experimental conditions, Section 4 describes data analysis. Section 5 summarizes the experimental results and considers phenomena relative to the accuracy of the data. Section 6 discusses the implication of this work for battery production and gives a procedure for estimating the amount of reaction that Li(Si) pellets undergo during production exposure. Finally, Section 7 briefly summarizes the major conclusions reached.

2. Experimental Procedure

The basic instrumentation used was a Perkin-Elmer Thermal-Analysis System 4 coupled with a flow system that allowed the generation of known water concentrations in a carrier gas. Samples were rapidly heated to a predetermined temperature; then weight versus time was plotted on a strip-chart recorder. The accuracy of the weight measurements was limited by

the uncertainty involved in reading the strip-chart trace, or about ± 0.002 mg (less than 1% on most data).

Figure 1 shows the pellet reacting in the instrument. Pellets were placed on a small pan attached to a microbalance and suspended in a cup-like arrangement with heating coils in the walls of the cup. The arrows trace the reacting gas flow.

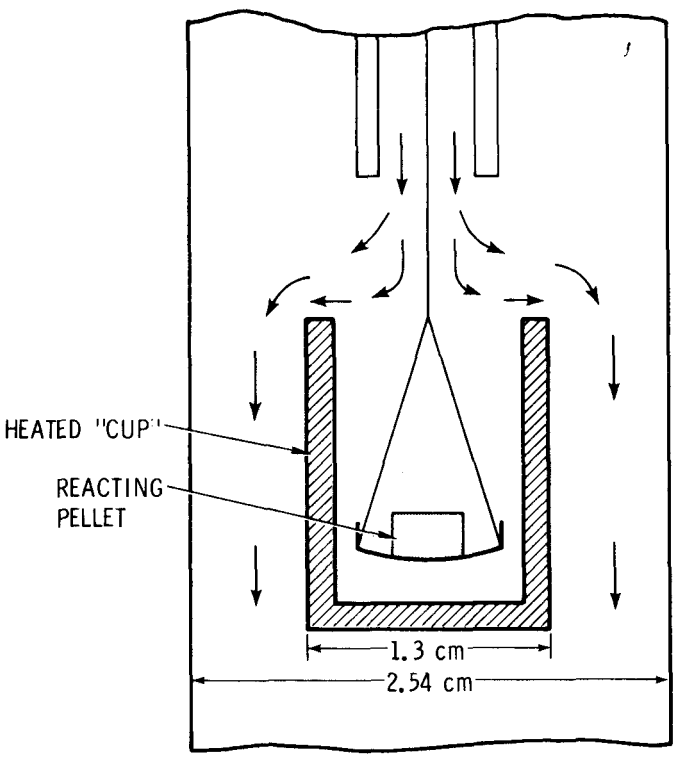

Figure 1. Reaction Volume

The flow system used to generate known quantities of water vapor in the carrier gas is illustrated in Figure 2. This system split the gas flow into two streams. One stream (designated as F_1) passed through a fritted disk immersed in a constant temperature bath stabilized at $2° \pm 0.3°C$. The gas flowing out of the water reservoir contained a partial pressure of water vapor equivalent to the equilibrium vapor pressure of

the water at 2°±0.3°C. The two gas streams, F_1 and F_2, were then mixed and passed over the Li(Si).

By using three assumptions (1) the ideal gas law, (2) a negligible pressure drop in the flow system, and (3) conservation of mass in the flow system, we can show that the water-vapor concentration above the Li(Si) in these experiments is given by the following equation.

$$C_{H_2O} = \frac{F_1}{F_1 + \left(\frac{P}{P_{wv}} - 1\right)\left(F_1 + F_2\right)} \left[\frac{P}{760} \cdot \frac{273}{T} \cdot \frac{18}{22\ 400}\right] . \qquad (1)$$

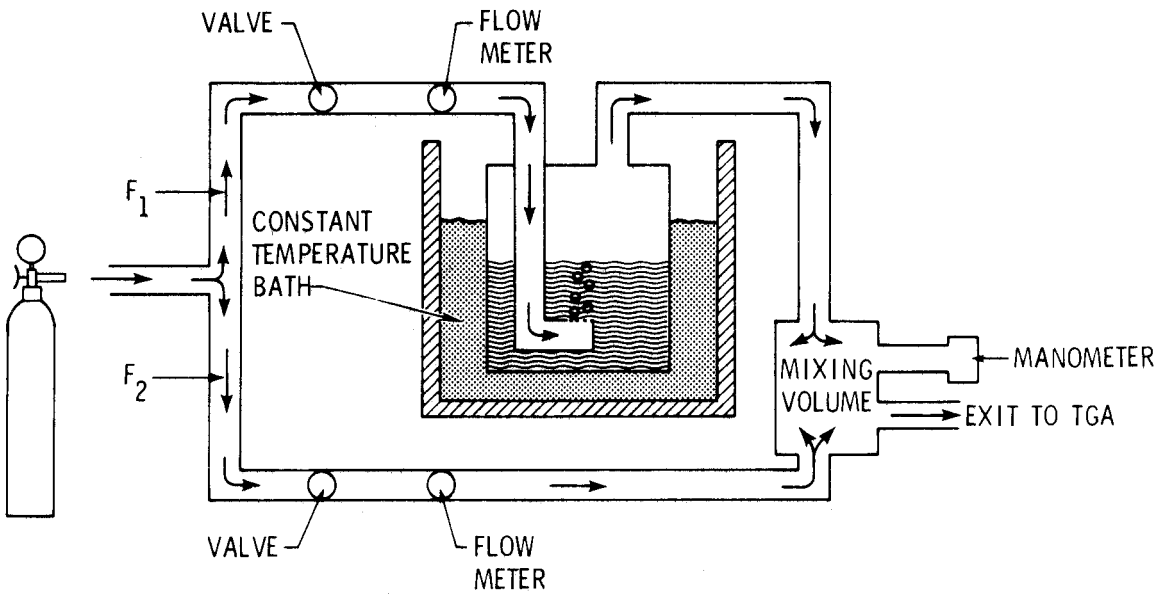

Figure 2. The Gas-Flow System Used to Generate Known Concentrations of Water Vapor in Various Carrier Gases

If it is assumed that $\frac{P}{P_{wv}} \gg 1$, this can be closely approximated by

$$C_{H_2O} = \frac{P_{wv}F_1}{F_1 + F_2} \left[\frac{1}{760} \cdot \frac{273}{T} \cdot \frac{18}{22\ 400}\right] \qquad (2)$$

or

$$C_{H_2O} = 2.89 \times 10^{-4} \frac{P_{wv}}{T} \left[\frac{F_1}{F_1 + F_2} \right] \tag{3}$$

where

C_{H_2O} = g/cm^3

P_{wv} = mm Hg

T = K

F1,F2 = cm^3/s.

All variables are defined in Appendix A.

In these experiments, the value of P_{wv} was taken[3] as 5.3±0.15 mm Hg. F_1 and F_2 were measured with two Manostat flowmeters. Calibration factors for determining the volume flow rate for a given reading were taken from the manufacturer's literature for each gas used. The overall uncertainty in calculating C_{H_2O} from the above equation is believed to be ~±7%.

In practice, it was necessary to flow gas through the system for several hours to purge it of other gases and allow all surfaces to reach equilibrium with the water vapor. A Panametrics Model 1000 hygrometer was incorporated in the system to monitor the water content of the exhaust gas. Experiments were run by quickly placing a pellet in the system after the hygrometer stabilized.

Weight-gain data were taken for Li(Si) samples (44 wt% Li) that were pressed into small pellets with the geometry shown in Figure 1. Pellets were made in a dry room (water content <300 ppm) and stored in a desiccator. The value of the radius for each pellet was assumed to be determined by the radius of the pelletizing fixture. The weight and height of a representative sample of pellets were carefully measured, and an average density of 0.97 g/cm^3 was calculated. This density value was used along

with the weight measured by the TGA and the known radius of the pelletizing fixture to determine the thickness (h) for each pellet.

It can be shown that for the given geometry

$$h = \frac{\text{mass of pellet}}{(\text{density})(\pi r^2)} = \frac{0.33\ W_i}{r^2} \tag{4}$$

The assumption that each pellet had the same density is not believed to be a source of significant error since all the pellets were made by the same operator using the same technique, and all pellets weighed about the same.

Data were generated for pure gases by isolating the water reservoir with shutoff valves. No attempt was made to dry the system thoroughly except for a purge of several hours that did not remove all the water vapor. Data will be discussed later that suggest the presence of water vapor in varying amounts in the system for <u>all</u> the so-called "pure" gases.

3. Applicable Reaction-Rate Models

The reaction of Li(Si) with any atmospheric gas is a heterogeneous reaction between a solid and a gas, and mass transport must be included as an integral part of the reaction-rate model. Reactions of this kind have been studied in the past and numerous descriptions published. The models used in this work were taken from the text by J. M. Smith.[4] An alternate discussion may be found in the book by Szekely, Evans, and Sohn.[5] These authors developed equations for pellets of spherical geometry, and their methods may be used to develop applicable equations for other geometries. In this work, data were generated with flat, round pellets; the necessary equations were accordingly developed for that geometry.

During this work we observed that water vapor reacted with Li(Si) only at exposed geometrical surfaces, while Li(Si) reacting with nitrogen and oxygen seemed to penetrate into the pellet to the surface of each

particle. Therefore two models (both termed "shrinking-core models") are necessary to adequately describe the reactions of Li(Si) with atmospheric gases. These models assume that no pellet volume change is associated with the reaction. In one model the reacting pellet is considered porous to the reacting gas; in the other case it is not. Even though a pellet is porous to inert gases, a reacting gas may not penetrate into the interior of the sample because of mass-transfer limitations.

Mathematical expressions are developed in the following paragraphs for the solid-core model with the pellet geometry. Certain assumptions and observations are made that allow transformation of the pellet geometry to a one-dimensional geometry. The one-dimensional geometry is then used with appropriate mass-transport equations and a first-order reaction-rate law to obtain a rate expression for the solid-core model. Finally, an expression is determined for the porous-core model in an analogous manner.

Figure 3 is a cross section of a flat, round pellet reacting according to the solid-core model. Note that reaction is not allowed on the bottom of the pellet since none was indicated in our experiments. The reacting gas (water vapor) diffuses from the surrounding medium to the surface of the pellet, then through a layer of reaction product to react in a zone assumed to be of zero thickness. A concentration gradient of the reacting gas exists in both the gas phase and the reacted solid phase (Figure 3). In this model it is assumed that any gas formed at the reaction front diffuses back out into the gaseous phase at a fast rate and contributes no net weight gain.

To facilitate the development of a rate expression for the solid-core model, it is desirable to transform the three-dimensional geometry shown in Figure 3 to a one-dimensional problem and also to develop equations that relate weight gain to the fraction of the material that has reacted. The system shown in Figure 3 can be transformed to a one-dimensional problem by defining "x" as the distance into the pellet perpendicular to the top surface and into the pellet along any radius. x_r is defined as the distance from any outside surface to the reaction front in the pellet.

The assumption is made that concentration effects at the top edge of the pellet have no significant impact on the reaction rate, and that reaction proceeds uniformly on all exposed geometrical surfaces. This model allows mass transport to the pellet in the gaseous phase and into the pellet along a single axis (x), and over a variable surface area.

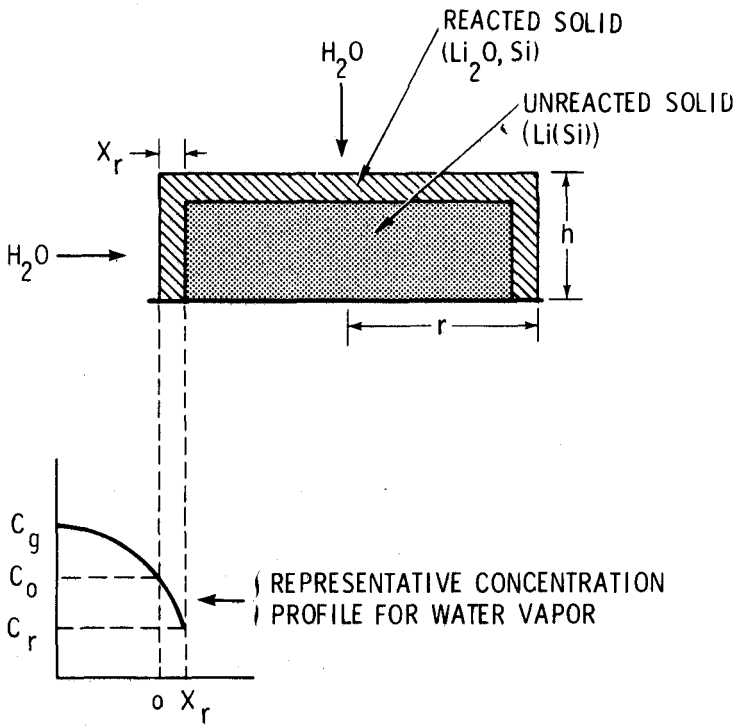

Figure 3. Shrinking Core Model With a Solid Core

An expression for x_r in terms of measured variables h, r, and weight gain can be determined if it is assumed that no volume change is associated with reaction, and if the reaction product is known. (All variables used are listed in Appendix A, and many are illustrated in Figure 3.) For water reacting with Li(Si), the only observed reaction product was Li_2O (see Section 5).

It can be easily shown that a 1 g sample of Li(Si) (44 wt%), which has reacted to form all Li_2O and silicon, will weigh 1.503 g. Therefore,

$$\frac{\text{pellet weight at time t - initial wt}}{\text{1.503 initial wt - initial wt}} = \frac{\text{volume reacted}}{\text{initial volume}}$$

or

$$\frac{\left(W_t - W_i\right)}{0.503\ W_i} = 1\ 988 \left[\frac{W_t}{W_i} - 1\right] = \frac{V_r}{V_i} . \tag{5}$$

The ratio of V_r to V_i can easily be expressed in terms of x_r by inspection of Figure 3, and this equation becomes

$$1.98\left[\frac{W_t}{W_i} - 1\right] = \frac{\pi r^2 h - \pi (r - x_r)^2 (h - x_r)}{\pi r^2 h} , \tag{6}$$

which can be rearranged to give Eq (7).

$$x_r^3 - x_r^2(h + 2r) + x_r(2rh + r^2) + 1.988r^2h\left[1 - \frac{W_t}{W_i}\right] = 0 \tag{7}$$

The area of the reaction zone (A_r) can also be determined by inspection of Figure 3, and it is given as Eq (8).

$$A_r = A_o - x_r(4\pi r + 2\pi h) + 3\pi x_r^2 \tag{8}$$

In order to describe the mass-transport and chemical-reaction rate for the one-dimensional representation of the system shown in Figure 3, it is necessary to assume existence of a steady state in which the mass of oxygen transported through the gas phase to the surface of the pellet exactly equals that transported through the reacted solid to the reaction front. In turn this mass of oxygen exactly equals the mass that adds to the weight of the pellet by reaction at the reaction front. Note that the oxygen is transported into the pellet as water vapor (therefore, mass-transport equations are written for water vapor), and hydrogen formed at the reaction front diffuses back out of the pellet. The steady-state

assumption allows the following three equations to be written:

$$1.13 \frac{dw}{dt} = A_0 \, k_g \, (C_g - C_o) \tag{9}$$

$$1.13 \frac{dw}{dt} = A_r \, k_s \left[\frac{dg}{dx}\right]_{x = x_r} \tag{10}$$

$$1.13 \frac{dw}{dt} = A_r \, k_r \, C_r \tag{11}$$

Equation (9) describes mass transport through the gas phase; Eq (10), mass transport through the reacted solid phase; and Eq (11), the reaction rate at the reaction front. The form of Eq (11) assumes a reaction that is first order with respect to water-vapor concentration. There is no a priori reason for choosing this rate expression for Eq (11) other than that but this functional form adequately fits our data. The constant 1.13 in these equations corrects the concentration term from grams of water vapor to grams of oxygen.

Equations (9), (10), and (11) can be solved simultaneously with appropriate boundary conditions (see Reference 4 for the general procedure) and the following equation results:

$$\frac{dw}{dt} = \frac{0.89 \, k_r k_g A_o A_r C_g}{A_r k_r + A_o k_g + \dfrac{A_r k_r A_o k_g F(x_r)}{k_s}} \tag{12}$$

where

$$F(x_r) = \frac{1}{\sqrt{-q}} \left[\ln \left(\frac{6\pi x_r - m - \sqrt{-q}}{6\pi x_r - m + \sqrt{-q}} \right) - \ln \left(\frac{m + \sqrt{-q}}{m - \sqrt{-q}} \right) \right]$$

and

$$m = 4\pi r + 2\pi h$$

$$q = 12\pi A_o - m^2 \, .$$

At zero time, $A_r = A_o$, $x_r = 0$, and the above equation reduces to Eq (13).

$$\left(\frac{dw}{dt}\right)_{t=0} = \frac{0.89}{k_r} \frac{k_r k_g}{+ k_g} A_o C_g \quad . \tag{13}$$

In the second reaction model used in this report, it is assumed that the reacting gas can penetrate the pellet, and that reaction occurs on all accessible surfaces. In those cases where this model applies, mass-transport limitations in the gas phase are rarely important, especially if the reacting gas is the major component in the gas phase. Forced convection occurs; this is a much faster transport mechanism than diffusion. Therefore, $k_g >> k_r$, and an equation analogous to Eq (13) can be written as:

$$\left(\frac{dw}{dt}\right)_{t=0} = k_r A_o' C_g \tag{14}$$

where A_o' is an effective specific surface area that is usually specified as area per unit mass of reacting solid. A_o' cannot be detemined a priori, and it may be included in the zero-time-rate constant as follows:

$$k'_{r,t=0} = \frac{k_r A_o'}{W_i}$$

Equation (14) then becomes

$$\left(\frac{dw}{dt}\right)_{t=0} = W_i \; k'_{r,}\left(t=0\right) C_g \tag{15}$$

The determination of an expression for dw/dt at nonzero times for the porous-core model requires further simplifying assumptions since an undefined reaction area is involved. In this report, because only zero-time-rate constants for this variation of the model are determined, no

further development of the mathematics will be given. Note that k_r' has units of volume/(mass · time), whereas k_r in other equations has units of length/time.

4. Data Analysis

In analyzing the data, we first assumed (as discussed in Section 3) that all data for water-vapor reaction followed the solid-core model, whereas the data for the pure gases followed the porous-core model. Data anlysis with the solid-core model was accomplished by using Eqs (12) and (13). Weight-gain data for a particular pellet were examined and the slope of the curve at zero time was estimated. This value was used in Eq (13) to determine a value for k_r, which in turn was used in Eq (12) along with measured slopes for the same pellet at various times to calculate a value for k_s. A value for x_r in Eq (13) was obtained by solving Eq (7) for x_r; A_r was obtained using Eq (8). Figure 4 gives an example of weight-gain data measured for a pellet. The straight lines used to determine dw/dt at zero time and at 2.8 h are also given.

The data analysis described above for the solid-core model required a value for the gas-phase mass-transport coefficient (k_g) for water vapor diffusing through the carrier gas. The gas flow shown in Figure 2 allows a possible stagnation region immediately above the reacting sample. In many of the experiments the flowing gas was at a substantially different temperature from that of the gas and sample inside the heated cup. No previous work was found that determined values for k_g for the flow situation described in Figure 2. However, approximations can be made by using empirical correlations if it is assumed that a nonturbulent flow exists in the system. This assumption is reasonable for those measurements in which the temperature of the reacting sample is not much different from that of the flowing gas. For data taken with a wide temperature difference between the flowing gas and the reacting sample, an assumption of turbulent flow is probably more valid. In turbulent flow, k_g becomes large and

the concentration at the surface of the pellet is closely approximated by the concentration of bulk gas.

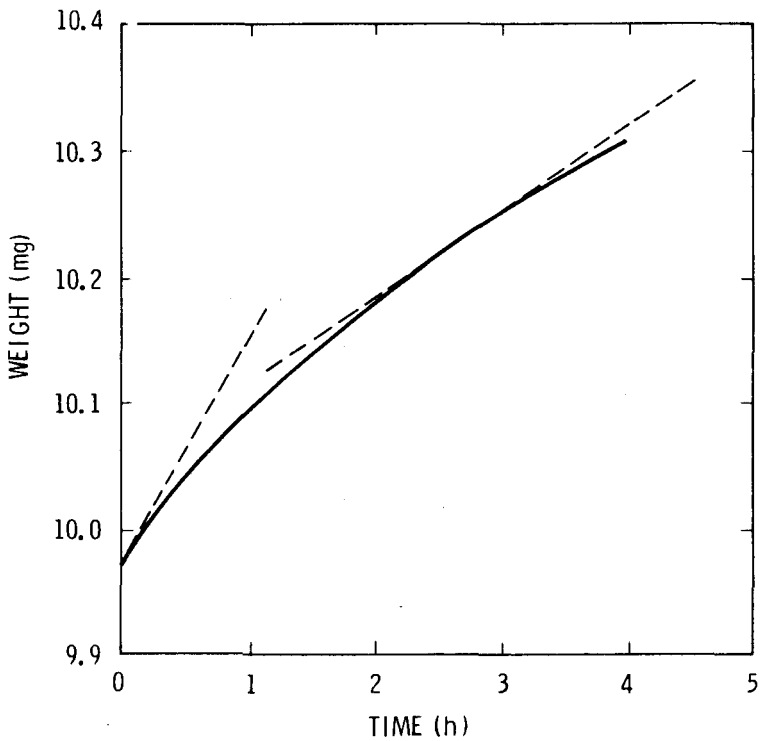

Figure 4. Data For a Pellet Exposed to 4.26×10^{-7} g/cm^3 Water Vapor in Argon Carrier Gas at 100°C. (Dotted lines indicated the slopes determined at time = 0, and time = 2.8 h.)

To determine values for k_g, the text by Smith[4] was followed closely, and the following equation was used.

$$k_g = j_D \, v\left(\frac{u}{\rho D}\right)^{-2/3} \tag{16}$$

To determine realistic values for the viscosity (u) and the diffusivity (D), a hard-sphere collision model was assumed.[6,7] This model predicts the following two equations.

$$D = \frac{3}{32} \frac{1}{N\sigma_{12}^{2}} \left(\frac{8kT}{\pi \frac{m_1 m_2}{m_1 + m_2}} \right)^{1/2} \tag{17}$$

and

$$u = \frac{m_2 kT}{\pi}^{1/2} \frac{1}{\pi \sigma_v^2} \tag{18}$$

The two equations can be simplified by substituting appropriate constants for the experimental conditions (average total pressure, 670-mm Hg); the following two equations are obtained:

$$D = 2.08 \times 10^{-3} \frac{(T)^{3/2}}{\sigma_{12}^{2}} \left(\frac{M_1 + M_2}{M_1 M_2} \right)^{1/2} \tag{19}$$

and

$$u = \frac{2.72 \times 10^{-5}}{\sigma_v^2} (M_2 T)^{1/2} \quad , \tag{20}$$

where M_1 and M_2 now refer to the molecular weight of water vapor and the carrier gas, respectively. Values of σ_{12}^2 and σ_v^2 in these equations are in square angstroms. These quantities represent collision cross sections determined from diffusion and viscosity data. Table 1 gives the values from References 6 and 7 that we used.

Table 1

Cross-Section Values

Carrier Gas	σ_{12}^2	σ_v^2
Argon	7.95	13.25
Nitrogen	8.01	14.06
Oxygen	7.56	13.03
Air	8.01	14.06

The density of the gas in these experiments is dominated by the carrier gas. A simple application of the ideal gas law allows the following expression for density in these experiments.

$$\rho = \frac{670}{760} \cdot \frac{273}{T} \cdot \frac{M_2}{22\ 400} = 1.07 \times 10^{-2}\left(\frac{M_2}{T}\right) \tag{21}$$

The three equations for diffusivity, viscosity, density, and an expression for v (determined from experimental conditions) were substituted into Eq (16) to obtain Eq (22).

$$k_g = j_D \left[\frac{F_1 + F_2}{3.8}\right] \left[1.22\ \frac{\sigma_{12}^2}{\sigma_V^2} \left(\frac{M_1}{M_1 + M_2}\right)^{1/2}\right]^{-2/3} \tag{22}$$

The constant j_D was determined by extrapolating the curve of j_D versus Reynold's number given on p 364 of Reference 3. (The characteristic dimension used in determining Reynold's number was the diameter of the cup in Figure 2, or 1.3 cm.)

For most of the data analysis that used the solid-core model, Eq (22) was used to calculate k_g. In one series of data it was assumed that gas-phase transport was not restrictive (i.e., turbulent flow with a very large k_g). The data for this series are listed in Table B-9, Appendix B.

For data generated with pure oxygen and nitrogen, Eq (15) was used to calculate a zero-time reaction-rate constant. The slope of the weight-gain data at zero time was used with this equation as explained above for the porous-core model illustrated in Figure 3.

5. Results

The tables in Appendix B summarize the data and results for all the weight-gain data. Values of k_r, k_s, k_g, and $k'_{r,t=0}$ for each experiment are listed in the tables. If it is assumed that k_r varies according to the Arrhenius form the following equation can be written:

$$k_r = B\, e^{-\frac{E}{1.98T}} \tag{23}$$

The standard procedure for using this functinal form is to plot $\ell n(k_r)$ versus $10^3/T$, and to determine the slope and intercept to evaluate E and B. In this work, a statistical curve-fitting program developed by Hewlett-Packard was used with an HP-67 calculator to determine B and E for each data set. The routine also determined a correlation factor (f^2) that indicates how well the data fits the functional form (a value of 1 would be a perfect fit). Values of B, E, and f^2 are given in the tables of Appendix B.

The results generated for the pure gases would fit the form only for higher temperatures. Figures 5 and 6 plot all the values for $k'_{r,t=0}$ determined for oxygen and nitrogen, respectively. A solid straight line on each of these figures gives the line generated by using the values of B and E in Tables A-1 and A-2, respectively.

The data generated for known amounts of water vapor can be used to calculate apparent values for $k'_{r,t=0}$ for a given water concentration. The dotted lines in Figures 5 and 6 represent the expected curve obtainable if the oxygen and nitrogen contained 5×10^{-8} g H_2O/cm^2 (about 70 ppm).

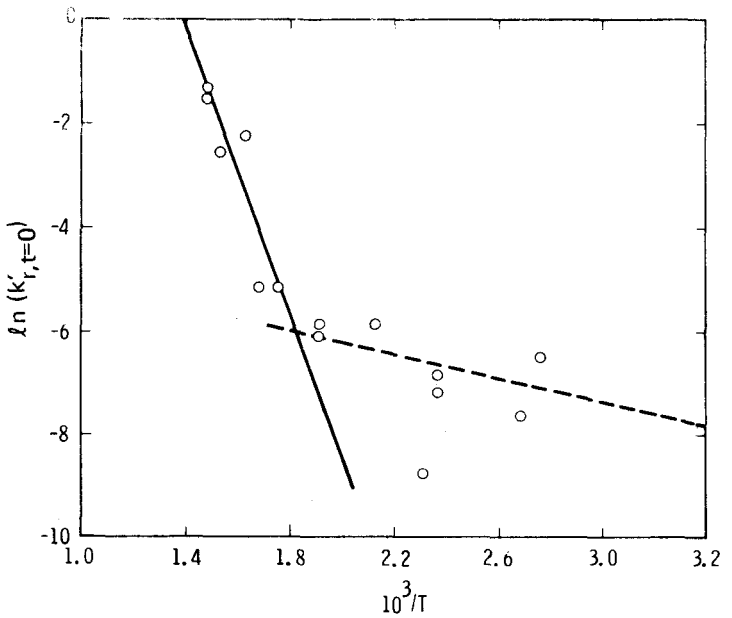

Figure 5. Plot of $\ell n(k'_{r,t=0})$ vs $10^3/T$ for the Data Generated With Oxygen Gas; No Water Vapor Added. (The solid line gives the best fit of the higher temperature data, and the dotted line gives the curve calculated for oxygen with 5 x 10^{-8} g/cm^3 water vapor, or about 70 ppm.)

Inspection of Figures 5 and 6 suggests that the data for lower temperatures more closely approximate the dotted line, while the higher temperature data clearly follow the solid line. The data for nitrogen begin following the solid line at temperatures >650K (~375°C), whereas the data for oxygen begin following the solid line at temperatures >550K (~275°C).

As previously stated, the so-called "pure" gases were contaminated by a variable amount of water vapor caused by evaporation off the walls of the flow system. Apparently, the weight gain at lower temperature in the pure gases was dominated by the reaction of Li(Si) with this residual water, since the rate constants more closely follow an expression generated for water-vapor data. Therefore, it is suggested that only the higher temperature data (solid lines) in Figures 5 and 6 represent the reaction of the pure gases with Li(Si).

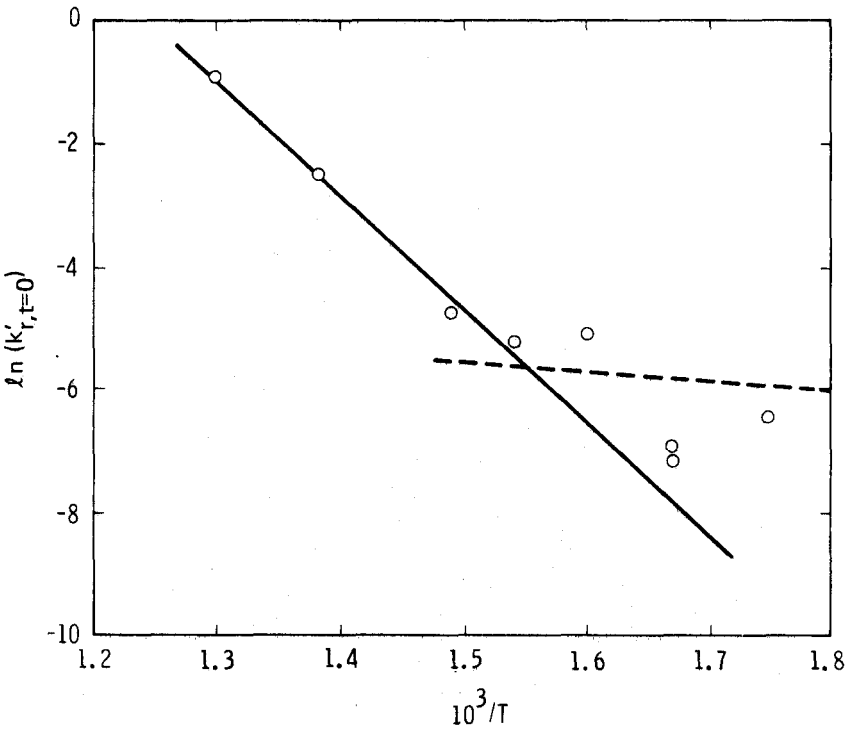

Figure 6. Plot of $\ell n(k'_{r,t=0})$ vs $10^3/T$ for the Data Generated With Nitrogen Gas; No Water Vapor Added. (The solid line gives the best fit of the high-temperature data; the dotted line gives the curve calculated for nitrogen with 5×10^{-8} g/cm^3 water vapor, or about 70 ppm.)

All the different values of k_r determined for water vapor are plotted in Figure 7. The solid line in this figure gives values of B = 55.5 and E = 3×10^3. Two sources of uncertainty contribute to the scatter in these data. First, the values used for k_g were not precise, as discussed in Section 4. Second, the initial condition of the pellet surfaces was not controlled. The data analysis assumes no reaction layer on the outside of the pellets at zero time, when in fact an oxide coating of unknown thickness was present. In order for this layer to have no impact on the chemical reaction rate as calculated, the mass transport through it would have to be much greater than the chemical reaction rate. The maximum thickness of the oxide layer that would satisfy this condition can

be approximated by using the values of k_s and k_r with Eq (24) and it is estimated that an oxide thickness of 2.5×10^{-5} cm would cause a 1% error. The pellets used in this work were exposed for variable time periods to dry-room conditions; it is not known if this condition was satisfied.

The pellets were handled more carefully than usual during battery production, and it is believed that reaction rates calculated using the resulting B and E will reflect the production situation.

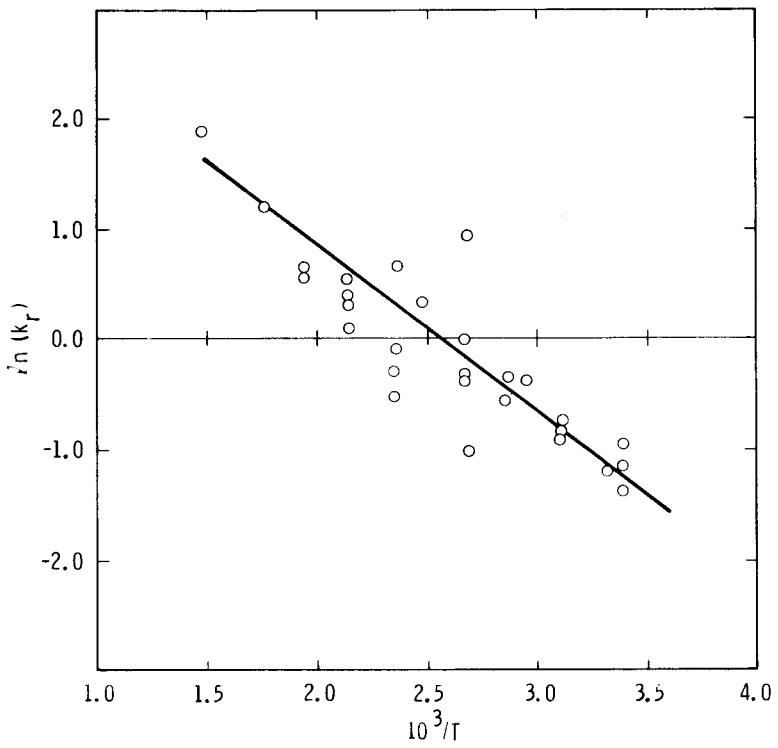

Figure 7. Plot of $\ell n(k_r)$ vs $10^3/T$ for All Water-Vapor Data. (Solid line gives values of B = 55.5 and $E = 3 \times 10^3$.)

Values of k_s determined in this work show more variability than values of k_r. In part, this is caused by the difficulty in accurately determining the slope of the weight versus the time curve at various times. However, k_s is a value that measures the resistance to mass flow through the reacted solid, and any phenomenon affecting mass transport

would have a large impact on k_s. Two phenomena affecting k_s are the thickness of the initial oxide layer, and any change in the density of the pellet or the particle size of the Li(Si) particles.

If k_s were truly a diffusivity, and if the data were accurate, k_s would vary according to the square root of temperature. Figure 8 plots k_s versus $T^{1/2}$. Although no clear trend is obvious from this graph, the values of k_s at temperatures near ambient seem to cluster between 5×10^{-4} and 1×10^{-3}. It is therefore suggested that the average, 7.5×10^{-4}, be used in calculations of reaction rate at ambient temperature.

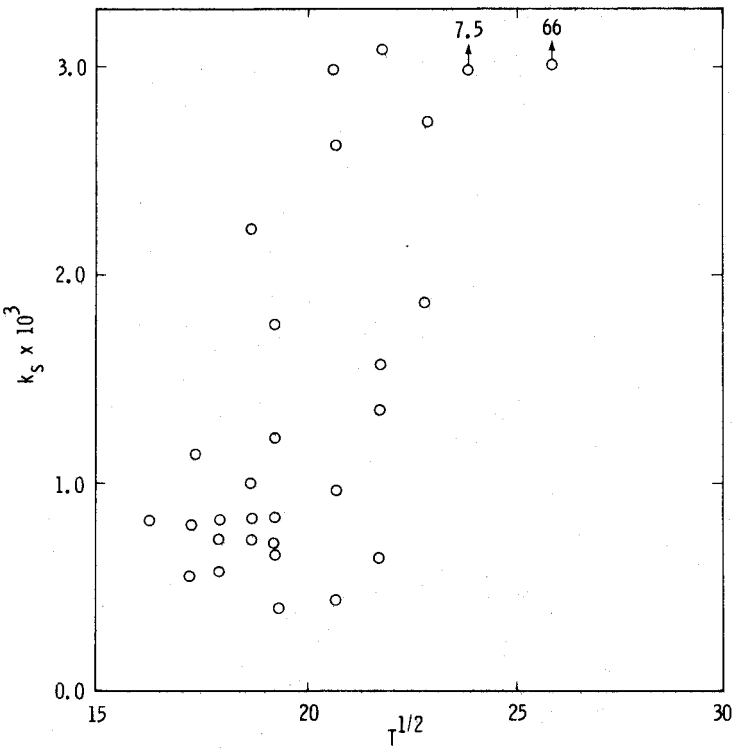

Figure 8. Plot of k_s vs $T^{1/2}$. (The two values indicated by arrows do not fit on this scale.)

G. C. Nelson (Division 5823) analyzed the pellets, using SIMS and ISS. All pellets contained substantial layers of lithium oxides and almost nothing else. The exceptions were those pellets exposed to nitrogen at higher temperatures that also had species in the surface layer with nitrogen atoms. The oxide layers on the pellets had various thicknesses,

but because the pellets were not labeled with respect to exposure time the layer thickness could not be correlated with other data.

Surface analytical data strongly support the conclusions that all data taken with pure carrier gases contained some water vapor, and that the major product on the pellets exposed to water vapor was lithium oxide. Presumably the hydrogen released by the reaction of Li(Si) with water vapor diffused back into the gas stream, and any hydroxide formed had been converted to lithium oxide by the time the pellets were analyzed.

6. Discussion

The generated data suggest that the reaction of Li(Si) with nitrogen and oxygen is insignificantly slow at temperatures prevalent during battery production and storage. However, Li(Si) reacts with water vapor very rapidly; the rate of this reaction should be used to specify handling procedures. No evidence exists to suggest that the reaction of Li(Si) with nitrogen was catalyzed by water vapor, however, this possibility was not adequately explored. No data points were taken at temperatures >300°C with water vapor in nitrogen, and the maximum water-vapor concentration used was ~1000 ppm. Catalysis of the Li(Si) reaction with nitrogen may not be apparent in these ranges of temperature and water-vapor concentration. The data clearly indicate that no significant catalytic effect is present at temperatures and water-vapor concentrations that are important in the production of thermal batteries.

To calculate the exact amount of reaction that a Li(Si) pellet would undergo, it is necessary not only to numerically integrate Eq (10) for every pellet geometry used, but also to have a good value of k_g and k_s. It is possible, however, to make certain simplifying assumptions and obtain a generalized result applicable to any pellet. Since the gas-phase mass-transport rate at ambient conditions does not have an overwhelming effect on the surface concentration (<30% error) for these experiments near ambient temperature, it can be assumed that k_g is very large.

Further, because most battery pellets have a radius much greater than their thickness, it can be assumed that $r \gg h$. It can be shown that if these two assumptions are allowed, Eq (10) is closely approximated by

$$\frac{dw}{dt} = \frac{0.89\ k_r A_o C_g}{1 + \frac{k_r}{k_s} x_r} \tag{24}$$

The integral of this equation between time limits of $t = 0$ and $t = t$ is equivalent to $W_t - W_i$. By retaining the assumption that $r \gg h$, setting $r = 0.56$ cm (radius of a unit area circle), assuming a pellet density of 0.97, and equating $W_t - W_i$ to the integral of Eq (23), we can show that Eq (7) reduces to

$$x_r^3 - 1.13\ x_r^2 + 0.318\ x_r - 0.643 \int_o^t \frac{dw}{dt} = 0 \tag{25}$$

Equation (24) can then be integrated numerically by solving for x_r (using Eq (25)) at each time increment. This integration predicts the weight gain per cm^2 of surface area for a sample of Li(Si) exposed to water vapor at concentration C_g.

Values of $(W_t - W_i)$ were calculated by using Eqs (24) and (25) for several of the TGA experiments and were compared to observed weight-gain data as a check on the validity of this approach. In these calculations k_r was determined by using Eq (23) and values of $B = 55.5$ and $E = 3 \times 10^3$. A value of 7.5×10^{-4} was used for k_s. Since values of C_o can easily be calculated for the experiments done in the TGA (using Eqs (8) and (22) with experimental data for the initial value of dw/dt), the water-vapor concentration at the surface of the pellet was used instead of C_g. The calculated curves agreed well with data like that in Figure 4 except that the calculated curve gained weight at a rate slightly greater than the measured curve. This is easily explained since the curves were calculated

by assuming a constant reaction area, whereas the actual reaction area, A_r, decreased with time.

As another check on the validity of the calculational procedure discussed above, a simple experiment was conducted and compared with calculated values. A humidity chamber was prepared by placing a saturated solution of LiCl in the bottom of a closed desiccator (with no desiccant). After the chamber sat over the weekend, six Li(Si) pellets were placed flat in a stainless-steel tray on the top shelf of the desiccator. After 25 hours, the average weight gain of the six pellets was 0.049 gram. Since the exposed surface of the pellets was 10 cm^2, this was equivalent to 0.0049 g/cm^2. To calculate the weight gain, it was assumed that the relative humidity in the chamber was 11% as previously reported,[8] and it was assumed that the temperature was a constant 22°C. The calculated weight gain with these values was 0.011 g/cm^2. The observation that the calculated value was about twice the measured value in this experiment is easily explained: (1) there was no circulation of air in the chamber, and (2) the calculation ignored mass transport limitations in the boundary layer above the pellets.

Figure 9 gives the integral of Eq (24) as a function of time for three different water-vapor concentrations. In order to display a greater range of data, the integral of dw/dt is plotted on a $\log_{10}$ scale. To use this figure, it is necessary to determine the total sur-face area in centimetres squared of an Li(Si) pellet that is exposed to the water vapor, and multiply by the value of ΔW determined from Figure 9 for the particular exposure time. ΔW is then added to the initial weight of the pellet to give its new weight. If a pellet gains 1.5 times its original weight, it has been completely converted to lithium oxide and silicon.

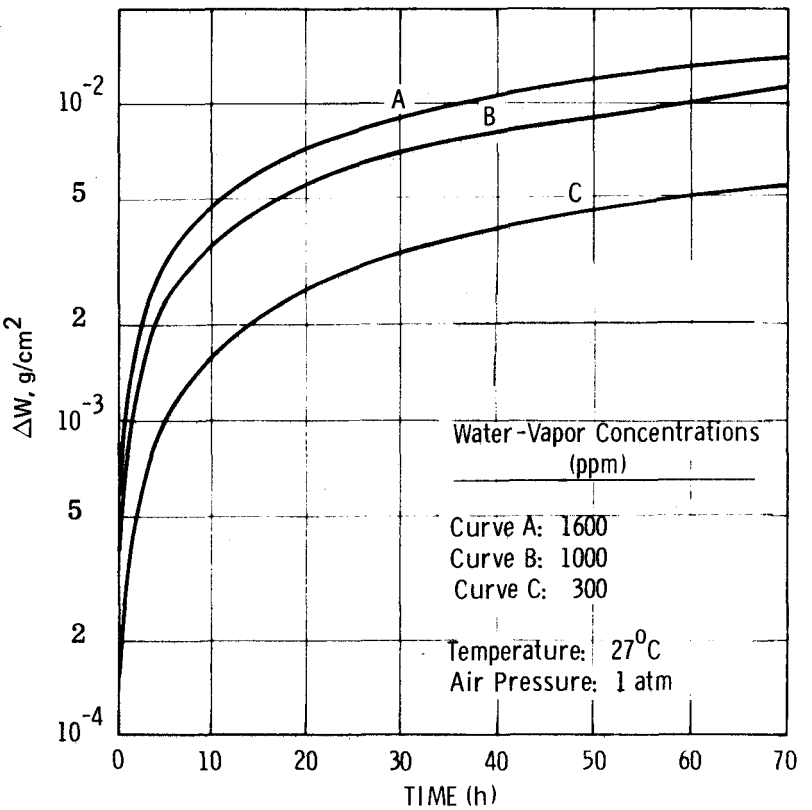

Figure 9. Calculated Curves for the Weight Gain per cm^2 of Li(Si) Pellet Exposed to Varying Water-Vapor Concentrations

Estimates of weight gain for Li(Si) pellets based on the curves given in Figure 9 are expected to be too large by 10% to 30% because of mass-transport limitations in the boundary layer immediately above the pellets. Loose-powder samples of Li(Si) are expected to have a larger value of k_s than the compacted pellets, but k_r should be the same in both cases. A larger value of k_s would predict a faster weight gain for the loose powder than that observed for pressed pellets. However, even a value of infinity for k_s would only double the value for the curves in Figure 9 at 5 h. Consequently, it is suggested that these curves be used to predict reaction of Li(Si) powder as well as pressed pellets for the relatively short exposure times that are important during battery production.

7. Conclusions

Li(Si) alloy with 44 wt% lithium reacts with oxygen and nitrogen at insignificantly slow rates under the conditions prevalent during the production and storage of thermal batteries. However, the same alloy reacts with water vapor so fast that the rate is inhibited by mass transport in the gas-phase boundary layer above the alloy. The reaction-rate model and data generated in this work allow calculation of the approximate weight gain of pellets and loose-powder samples of Li(Si) alloy for the ambient conditions of battery production.

References

[1]M. M. Markowitz and Daniel A. Boryta, "Lithium Metal - Gas Reactions," J of Chem and Eng Data, 7(4):586-591, October 1967.

[2]R. A. Sharma and R. M. Seeforth, "Thermodynamic Properties of the Lithium-Silicon System," J of the Electrochem Soc, 123(12):1763-1768, December 1976.

[3]Handbook of Chemistry and Physics (Cleveland, OH: Chemical Rubber Company, published yearly).

[4]J. M. Smith, Chemical Engineering Kinetics (New York: McGraw-Hill Book Co., 1970).

[5]J. Szekely, J. W. Evans, and H. Y. Sohn, Gas-Solid Reactions (New York: Academic Press, 1976).

[6]S. W. Benson, The Foundations of Chemical Kinetics (New York: McGraw-Hill Book Co., 1960).

[7]J. O. Hirshfelder, C. F. Curtis, and R. B. Bird, Molecular Theory of Gases and Liquids (New York: John Wiley and Sons, Inc., 1954).

[8]C. P. Hedlin and F. N. Trofimenkoff, "Relative Humidities Over Saturated Solutions of Nine Salts in the Temperature Range from 0° to 90°F," Humidity and Moisture, ed Arnold Wexler, vol. III, pp 519-520 (New York: Reinhold Publishing Corp., 1963).

APPENDIX A

List of Variables

APPENDIX A

List of Variables

A_o	Area of pellet exposed to water vapor (cm^2)
A'_o	Effective specific surface area for reaction of Li(Si) with pure gases (cm^2/g)
A_r	Total area of reaction front (cm^2)
B	Preexponential constant in Arrhenius equation
C	Concentration (g/cm^3)
C_g	Concentration of reacting species in the reaction volume (g/cm^3)
C_{H_2O}	Concentration of water vapor (g/cm^3) in the reaction volume
C_o	Concentration of water vapor at the pellet surface (g/cm^3)
C_r	Concentration of water vapor at the reaction front (g/cm^3)
D	Diffusivity of water vapor in carrier gas (cm^2/s)
E	Activation energy for rate constant (calories)
f^2	Statistical correlation factor
F_1	Flow rate of carrier gas through water reservoir (cm^3/s)
F_2	Flow rate of second carrier gas stream (cm^3/s)
h	Pellet height (or length) (cm)
j_D	Dimensionless constant (Chilton Colburn coefficient)
k_g	Mass-transport coefficient for water vapor in carrier gas (cm/s)
k_r	Reaction rate constant for water vapor with Li(Si) at the reaction front (cm/s)
$k'_{r,t=0}$	Zero-time reaction-rate constant for pure gases with Li(Si) (cm^3/g-s)

k_s	Diffusivity of water molecules in the reacted solid (cm^2/s)
m_1	Molecular mass of water (g)
m_2	Molecular mass of carrier gas (g)
M_1	Molecular weight of water
M_2	Molecular weight of carrier gas
N	Molecular number density (molecules/cm^3)
P	Pressure (mm Hg)
P_{wv}	Water-vapor pressure (mm Hg)
r	Pellet radius (cm)
t	Time (s)
T	Temperature (K)
u	Viscosity of flowing gas (g/cm-s)
v	Specific flow velocity of gas in thermal analysis instrument (cm/s)
V_i	Initial pellet volume (cm^3)
V_r	Volume of pellet that has reacted (cm^3)
W_i	Pellet mass at zero time (g)
W_t	Pellet mass at time t (g)
x_r	Distance from external pellet surface into the pellet to the reaction front (cm)
ρ	Density of gas phase (g/cm^3)
σ_{12}^2	Diffusion cross section for water vapor in carrier gas (A^2)
σ_v^2	Viscosity cross section of carrier gas (A^2)

APPENDIX B

Tables of Data and Results

Table B-1

Results for Samples Exposed to Oxygen

(Pellet Diameter = 0.45 cm)

W_i (g)	T (K)	$dw/dt_{t=0}$	C_g	k_r'
9.567×10^{-3}	373	5.0×10^{-9}	9.22×10^{-4}	5.67×10^{-4}
10.274×10^{-3}	473	1.14×10^{-8}	7.27×10^{-4}	1.53×10^{-4}
9.957×10^{-3}	573	3.28×10^{-8}	6.00×10^{-4}	5.49×10^{-3}
10.117×10^{-3}	423	8.89×10^{-9}	8.13×10^{-4}	1.08×10^{-3}
9.348×10^{-3}	373	3.89×10^{-9}	9.22×10^{-4}	4.51×10^{-4}
9.689×10^{-3}	523	1.61×10^{-8}	6.58×10^{-4}	2.53×10^{-3}
9.59×10^{-3}	423	5.77×10^{-9}	8.13×10^{-4}	7.4×10^{-4}
9.356×10^{-3}	473	1.72×10^{-8}	7.27×10^{-4}	2.53×10^{-3}
10.078×10^{-3}	523	1.58×10^{-8}	6.58×10^{-4}	2.38×10^{-3}
*10.464×10^{-3}	598	3.56×10^{-8}	5.75×10^{-4}	5.92×10^{-3}*
* 9.928×10^{-7}	623	1.08×10^{-7}	5.52×10^{-4}	1.97×10^{-2}*
*10.149×10^{-3}	648	4.06×10^{-7}	5.31×10^{-4}	7.40×10^{-2}*
* 9.86×10^{-3}	673	8.58×10^{-7}	5.11×10^{-4}	0.170*
* 4.76×10^{-3}	673	4.92×10^{-7}	5.11×10^{-4}	0.202*

B	2.01×10^{11}
E	36.89×10^{3}
f^2	1.00

*Values used to determine B and E

Table B-2

Results for Samples Exposed to Nitrogen

(Pellet Diameter = 0.45 cm)

W_i (g)	T (K)	$dw/dt_{t=0}$	C_g	k'_r
9.97×10^{-3}	573	8.30×10^{-9}	5.23×10^{-4}	1.60×10^{-3}
9.876×10^{-3}	598	4.70×10^{-9}	5.02×10^{-4}	9.50×10^{-4}
9.342×10^{-3}	598	3.90×10^{-9}	5.02×10^{-4}	8.32×10^{-4}
9.7×10^{-3}	623	2.61×10^{-8}	4.81×10^{-4}	5.76×10^{-3}
10.225×10^{-3}	648	2.58×10^{-8}	4.63×10^{-4}	5.45×10^{-3}*
10.31×10^{-3}	673	3.77×10^{-8}	4.46×10^{-4}	8.2×10^{-3}*
9.63×10^{-3}	723	4.28×10^{-7}	4.15×10^{-4}	0.107*
9.072×10^{-3}	773	1.40×10^{-6}	3.88×10^{-4}	0.398*

B	9.24×10^{9}
E	36.42×10^{3}
f^2	0.98

*Values used to determine B and E

Table B-3

Results for Samples Exposed to Water Vapor in Air

(Pellet Diameter = 0.45 cm; F_1 = 0.13; F_2 = 1.50)

W_i (g)	T (K)	$dw/dt_{t=0}$	j_D	k_g	k_r	k_s
9.7×10^{-3}	295	3.055×10^{-8}	1.4	1.38	0.43	8.0×10^{-4}
10.7×10^{-3}	323	3.42×10^{-8}	1.54	1.52	0.52	5.7×10^{-4}
9.52×10^{-3}	348	5.8×10^{-8}	1.66	1.64	1.19	2.13×10^{-3}
10.35×10^{-3}	373	6.61×10^{-8}	1.79	1.76	1.63	1.76×10^{-3}

B	359.2
E	4.01×10^3
f^2	0.92

Table B-4

Results for Samples Exposed to Water Vapor in Oxygen

(Pellet Diameter = 0.45 cm; F_1 = 0.12; F_2 = 0.94)

W_i (g)	T (K)	$dw/dt_{t=0}$	j_D	k_g	k_r	k_s
9.652×10^{-3}	323	3.92×10^{-8}	2.11	1.04	0.46	8.4×10^{-4}
9.66×10^{-3}	348	5.25×10^{-8}	2.27	1.12	0.78	8.4×10^{-4}
9.54×10^{-3}	373	6.06×10^{-9}	2.44	1.20	1.12	1.2×10^{-3}

B	365.6
E	4.26×10^3
f^2	1.00

Table B-5

Results for Samples Exposed to Water Vapor in Nitrogen

(Pellet Diameter = 0.45 cm; F_1 = 0.13; F_2 = 1.52)

W_i (g)	T (K)	$dw/dt_{t=0}$	j_D	k_g	k_r	k_s
9.642×10^{-3}	302	2.3×10^{-8}	1.44	1.09	0.34	1.14×10^{-3}
9.838×10^{-3}	295	2.06×10^{-8}	1.41	1.07	0.28	8.45×10^{-4}
10.49×10^{-3}	343	2.61×10^{-8}	1.64	1.24	0.77	7.04×10^{-4}
9.755×10^{-3}	403	5.39×10^{-8}	1.94	1.47	1.61	2.56×10^{-3}

B	194
E	3.8×10^3
f^2	1.00

Table B-6

Results for Samples Exposed to Water Vapor in Nitrogen

(Pellet Diameter = 0.45 cm; F_1 = 0.13; F_2 = 4.58)

W_i (g)	T (K)	$dw/dt_{t=0}$	j_D	k_g	k_r	k_s
10.39×10^{-3}	373	1.25×10^{-8}	0.88	1.90	0.63	4.0×10^{-4}
9.756×10^{-3}	423	1.42×10^{-8}	1.00	2.16	0.84	9.6×10^{-4}
9.34×10^{-3}	473	1.61×10^{-8}	1.12	2.42	1.19	1.35×10^{-3}
9.23×10^{-3}	523	2.19×10^{-8}	1.24	2.68	2.15	2.72×10^{-3}

B	35.0
E	3.03×10^3
f^2	0.93

Table B-7

Results for Samples Exposed to Water Vapor in Argon

(Pellet Diameter = 0.45 cm; F_1 = 0.11; F_2 = 3.81)

W_i (g)	T (K)	$dw/dt_{t=0}$	j_D	k_g	k_r	k_s
10.2×10^{-3}	523	2.14×10^{-8}	1.29	2.42	2.02	1.86×10^{-3}
10.393×10^{-3}	473	1.97×10^{-8}	1.17	2.15	1.57	6.43×10^{-4}
10.0×10^{-3}	423	1.53×10^{-8}	1.04	1.95	0.97	4.3×10^{-4}
9.030×10^{-3}	373	8.33×10^{-9}	0.92	1.73	0.40	6.7×10^{-4}

B	126.1
E	4.18×10^3
f^2	0.97

Table B-8

Results for Samples Exposed to Water Vapor in Argon

(Pellet Diameter = 0.45 cm; F_1 = 0.11; F_2 = 0.95)

W_i (g)	T (K)	$dw/dt_{t=0}$	j_D	k_g	k_r	k_s
9.98×10^{-3}	373	4.75×10^{-8}	2.24	1.14	0.82	8.01×10^{-4}
9.2×10^{-3}	423	7.17×10^{-8}	2.54	1.29	2.25	2.98×10^{-3}
9.762×10^{-3}	296	3.05×10^{-8}	1.79	0.91	0.35	5.5×10^{-4}
10.44×10^{-3}	323	3.55×10^{-8}	1.93	0.98	0.45	7.4×10^{-4}
10.0×10^{-3}	348	4.19×10^{-8}	2.08	1.06	0.63	1.0×10^{-3}

B	124.6
E	3.55×10^3
f^2	0.93

Table B-9

Results for Samples Exposed to Water Vapor in Argon

(Pellet Diameter = 0.31 cm; F_1 = 0.11; F_2 = 0.95)

W_i (g)	T (K)	$dw/dt_{t=0}$	j_D	k_g	k_r	k_s
9.309×10^{-3}	673	3.3×10^{-7}	*	*	7.84	
9.64×10^{-3}	673	3.43×10^{-7}	*	*	7.97	6.64×10^{-2}
9.278×10^{-3}	573	1.83×10^{-7}	*	*	3.70	7.5×10^{-3}
9.868×10^{-3}	473	1.18×10^{-7}	*	*	1.90	3.09×10^{-3}
8.95×10^{-3}	473	9.89×10^{-8}	*	*	1.68	1.56×10^{-3}
9.152×10^{-3}	373	5.75×10^{-8}	*	*	0.76	6.7×10^{-4}

B	137.9
E	3.95×10^3
f^2	0.98

*Data analysis assumed turbulent flow, $k_g >> k_r$

DISTRIBUTION:

Harry Diamond Labs (2)
2800 Powder Mill Rd
Adelphi, MD 20783
Attn: A. Benderly
W. E. Kuper

Naval Surface Weapons Center (2)
Silver Spring, MD 20910
Attn: B. Larrick
C. E. Mueller

Navy Weapons Center (2)
China Lake, CA 93555
Attn: L. D. Pracchia
A. N. Fletcher

General Electric Co (10)
Neutron Devices Dept
P.O. Box 11508
St Petersburg, FL 33733
Attn: R. D. Walton
R. Szwarc
M. Osborne
J. Neale
R. A. Fleming
J. D. Sgro
J. R. Foley
B. Poole
R. Anteperko
W. Welbon

Frank J. Seiler Research Lab
FJSRL/NC
US Air Force Academy
Colorado Springs, CO 80840
Attn: Lt. Col. L. A. King

US Army Electronics Command
Ft. Monmouth, NJ 07783
Attn: D. Linden

Royal Aircraft Establishment
Materials Dept
Farnbrough, Hants, England
Attn: A. Attwell

Gould Inc.
40 Gould Center
Rolling Meadows, IL 6008
Attn: B. Askew

Eagle-Picher Industries, Inc (4)
Electronics Div, Couples Dept
P.O. Box 47
Joplin, MO 64802
Attn: R. Cottingham
R. Hudson
J. DeGruson
F. Smith

Eureka-Williams Co
Advanced Science Div
1201 E. Bell St
Bloomington, IL 61701
Attn: L. Raper

KDI Score, Inc
200 Wright Ave
Cockeysville, MD 21030
Attn: K. K. Press

Argonne National Lab (3)
9700 South Cass Ave
Argonne, IL 60439
Attn: R. K. Steunenberg
M. F. Roche
D. R. Vissers

Army Materiels and Mechanics (2)
Research Center
Watertown, MA 02172
Attn: J. W. McCauley
P. Wong

USA ARRADCOM-DRDAR-LCE
LCWSL EMD B1515
Dover, NJ 07801
Attn: B. Werbel

Atomics International
8900 DeSoto Ave
Canoga Park, CA 91304
Attn: L. McCoy

AF Materials Lab/LTM
Manufacturing Technology Div
Metals Branch
Wright-Patterson AFB, OH 45433
Attn: Maj. J. K. Erbacher

DISTRIBUTION (cont):

Admiralty Marine Tech Establishment (2)
Pouge, Dorset, England BH16JU
Attn: L. Pierce
R. T. M. Fraser

Catalyst Research Corp
1421 Clarkview Rd
Baltimore, MD 21209
Attn: F. Tepper

AF Aero Propulsion Labs
Aerospace Power Div
Wright-Patterson AFB, OH 45433
Attn: R. A. Marsh

Department of the Navy
Naval Weapons Support Center
Crane, IN 47522
Attn: L. Plew, Code 3073

Arthur D. Little, Inc
Acorn Park
Cambridge, MA 02140
Attn: J. Parry

Naval Sea Systems Command (2)
Attention Code SEA63R-32
Washington, DC 20235
Attn: M. F. Murphy
F. Butler

Naval Underwater Systems Center
Code 36301
Newport, RI 02840
Attn: R. S. Lazar

University of Arizona
Dept of Chemistry
Tucson, AZ 85721
Attn: N. R. Armstrong

Picatinny Arsenal (2)
Dover, NJ 07801
Attn: A. E. Magistro
M. R. Merriman

2500 J. C. Crawford
2510 D. H. Anderson
Attn: W. G. Perkins
B. H. Van Domelen
P. D. Wilcox
2520 H. J. Saxton
Attn: C. P. Ballard
A. L. Thornton
2522 R. D. Wehrle
Attn: A. H. Andazola
C. O. Weaver
R. C. Zaluga
2522 E. V. Forsman
2522 K. R. Grothaus
2523 R. K. Quinn
2523 J. R. Armijo
2523 A. R. Baldwin
2523 J. C. D'Angelo
2523 P. A. Neiswander
2523 F. W. Reinhardt (5)
2523 J. Q. Searcy (25)
2525 R. P. Clark
4332 K. D. Hardin
4363 J. Wagner
5815 R. T. Johnson
5820 R. E. Whan
Attn: K. H. Eckelmeyer
5821 N. E. Brown
Attn: R. W. Bild
R. M. Merrill
J. F. Wolcott
5823 J. A. Borders
Attn: G. C. Nelson
5832 R. W. Rohde
Attn: M. M. Karnowsky
R. J. Salzbrenner
5840 N. J. Magnani
Attn: R. J. Eagan
5841 D. W. Schaefer
Attn: B. C. Bunker
W. H. Smyrl
5846 E. K. Beauchamp
Attn: W. F. Hammetter
8153 J. B. Wright
Attn: L. E. Dighton
J. A. W. Kersey
8310 D. M. Schuster
8313 D. A. Nissen
8461 R. J. Bedford
8214 P. A. Childers
3141 T. L. Werner (5)
3151 W. L. Garner (3)
For DOE/TIC (Unlimited Release)
DOE/TIC (25)
(J. Hernandez, 3154-4)